

X-Ray Spectroscopy in the Microcalorimeter Era. I. Effects of Fe XXIV Resonant Auger Destruction on Fe XXV K α Spectra

P. Chakraborty, G. J. Ferland, M. Chatzikos, F. Guzmán, and Y. Su University of Kentucky, Lexington, KY, USA Received 2020 June 19; revised 2020 July 26; accepted 2020 July 30; published 2020 September 23

Abstract

We discuss the importance of Fe^{23+} in determining the line intensities of the Fe XXV K α complex in an optically thick cloud, and investigate resonant auger destruction (RAD) with CLOUDY. Although initially motivated by the Perseus cluster, our calculations are extended to the wide range of column densities encountered in astronomy. A Fe XXV line photon can change/lose its identity upon absorption by three-electron iron as a result of "line interlocking." This may lead to the autoionization of the absorbing ion, ultimately destroying the Fe XXV K α photon by RAD. Out of the four members in the Fe XXV K α complex, a significant fraction of the x line photons are absorbed by Fe^{23+} and destroyed, causing the x line intensity to decrease. For example, at a hydrogen column density of 10^{25} cm⁻², \sim 32% of x photons are destroyed due to RAD while w is mostly unaffected. The line intensity of y is slightly (\leq 2%) reduced. z is not directly affected by RAD, but the contrasting behavior between z and x line intensities points toward the possible conversion of a tiny fraction (\sim 2%) of x photons into z photons. The change in line intensities due to electron scattering escape off fast thermal electrons is also discussed.

Unified Astronomy Thesaurus concepts: Galaxy clusters (584); X-ray astronomy (1810); High resolution spectroscopy (2096); Radiative transfer (1335); Intracluster medium (858); X-ray observatories (1819)

1. Introduction

The Fe XXV $K\alpha$ complex has been a subject of interest in the X-ray community for decades. Observations of the Perseus cluster by Ariel 5 detected an emission feature near 7 keV caused by transitions from Fe XXV and Fe XXVI (Mitchell et al. 1976). The Fe XXV $K\alpha$ complex was later detected at 6.7 keV by XMM-Newton (Churazov et al. 2004). Recently, the Soft X-ray Spectrometer (Kelley et al. 2016) on board Hitomi resolved the complex into four components—the resonance (w), intercombination (x,y), and forbidden (z) lines (Hitomi Collaboration et al. 2016). Some previous studies of X-ray emission from He-like iron are by Bautista & Kallman (2000) and Mehdipour et al. (2015), and for lighter elements by Porquet & Dubau (2000) and Smith et al. (2001).

In the higher column density limit, two atomic processes contribute to the change in intensity of line photons in the Fe XXV K α complex. First, line photons are absorbed by satellites of three- electron iron and He-like chromium due to line interlocking and lose their identities (see Sections 4, 5). Second, Lyman line photons are absorbed by Fe XXV itself following the emission of different line photons (Case A to B transition), as discussed in the second paper of this series, Chakraborty et al. (2020, hereafter Paper II). However, it is difficult to decouple these two processes and study them independently. We focus this paper on the importance of line interlocking in deciding Fe XXV K α line intensities using the spectral synthesis code CLOUDY (Ferland et al. 2017), with occasional references to the Case A to B transition.

We also explore the effects of resonant auger destruction (RAD), line absorption by satellites leading to autoionization (Ross et al. 1978; Band et al. 1990). The term RAD was introduced by Ross et al. (1996) and more recently has been reviewed by Liedahl (2005). Although we do all our calculations using the physical parameters for the Perseus core, which is optically thin for x, y, and z, RAD only becomes important in the high-column-density limit. This is a spectral analysis in the column density parameter space,

extended up to the hydrogen column density $N_{\rm H}=10^{25}\,{\rm cm}^{-2}$, typically encountered in astronomy. Although such high column densities do not occur in the Perseus intracluster medium, they do happen in other environments, such as accretion disks, Comptonthick regions, Fe K α fluorescent emission lines in active galactic nuclei (AGNs), and some Seyfert galaxies (Matt et al. 1996; Bianchi & Matt 2002; Bianchi et al. 2005; Yaqoob & Murphy 2011; Yaqoob 2012; Marin et al. 2013; Tzanavaris et al. 2019), which CLOUDY can model. We document the full physical treatment for future reference.

In addition, at hydrogen column densities higher than $N_{\rm H}=10^{23}\,{\rm cm}^{-2}$, electron scattering opacity starts to become important. Line photons scatter off thermal electrons and become heavily Doppler-shifted, leading to one-scattering escape. We call this process electron scattering escape (ESE). This causes a deficit in the line intensity at the wavelength of the scattered photons. We elaborate on this process in Section 7.

This paper is organized as follows. Section 2 lists the various atomic data sources used in our calculations. Section 3 discusses the parameters used for our simulations with CLOUDY. Section 4 discusses the physics of line interlocking. Section 5 demonstrates autoionization following the absorption of Fe XXV K α line photons. Section 6 discusses the spectroscopic evidence of RAD in selective Fe XXV K α line photons. Section 7 describes the change in Fe XXV K α line intensities due to ESE. Section 8 summarizes our results.

2. Atomic Data

This section describes the various atomic data sources we use in our spectral modeling. Our calculations are very wavelength-sensitive and require a precise atomic data set for the accurate prediction of spectral behavior in the high-column-density limit. Atomic data sources for He-like iron (Fe²⁴⁺) are discussed in Paper II. Atomic data sources for the two ions contributing to line interlocking with Fe²⁴⁺, Fe²³⁺, and Cr²²⁺

Table 1

Energy Level Configurations, Labels, Corresponding Wavelengths, Downward Transition Probabilities $(A_{u,l})$, and Autoionization Rates (A_a) (if Applicable) for Transitions from the Ground in Fe²⁴⁺ Generating Fe XXV K α Complex, and in Fe²³⁺, Fe²²⁺, and Cr²²⁺ in the Proximity of the Fe XXV K α Complex

Ion	Configuration	Label	$Wavelength(\mathring{A})$	$A_{u,l}(s^{-1})$	$A_a(s^{-1})$
	1s.2p ¹ P ₁	W	1.8504	4.54e+14	
Fe ²⁴⁺	$1s.2p^{-3}P_2$	X	1.8554	6.30e+09	
	$1s.2p^{-3}P_1$	y	1.8595	4.11e+13	
	$1s.2s^{-3}S_1$	Z	1.8682	2.15e + 08	
	1s.2s.2p ² P _{3/2}	•••	1.8563	3.420e+12	1.09e+14
Fe ²³⁺	$1s.2s.2p^{-2}P_{1/2}$		1.8571	1.900e+14	7.58e+13
	$1s.2s.2p^{-2}P_{3/2}$		1.8610	4.680e + 14	2.90e+09
	$1s.2s.2p^{-2}P_{1/2}$		1.8636	2.920e+14	3.38e + 13
Cr ²²⁺	1s.3p ¹ P ₁		1.8558	8.970e+13	
Fe ²²⁺	1s.2s2.2p ¹ P ₁		1.8704	4.210e+14	5.56e+12

(for hydrogen column densities higher than $10^{23}\,\mathrm{cm}^{-2}$) are discussed below.

2.1. Energy Levels

The previous version of CLOUDY (Ferland et al. 2017) used Fe²³⁺ and Cr²²⁺ energy levels calculated using the code Autostructure, as described in Badnell et al. (2005). We replace these with CHIANTI version 9.0 (Dere et al. 1997, 2019), which uses a more recent Autostructure calculation (Badnell 2011). The process of "line interlocking" described in Section 4 is very sensitive to the line wavelengths, as even a slight variation in the energy levels can significantly change the line-center optical depths. We find that the uncertainty in Fe²³⁺ is particularly important for our analysis. See Section 8 for a brief discussion on how uncertainties in energy levels or velocity fields can alter the nature of the spectra in high column densities.

2.2. Transition Probabilities

For transitions between autoionizing levels and ground in Fe^{23+} , we use transition probabilities from CHIANTI version 9.0, which are taken from Autostructure calculations. Table 1 gives the list of transition probabilities used in our calculation near the energy range of the Fe XXV $K\alpha$ complex. We found a swap between two Fe XXIV lines in the NIST atomic database (Kramida et al. 2018), which can significantly alter the linecenter optical depth in x, as well as the calculations for RAD. This issue is further addressed in Section 8.

2.3. Autoionization Rates

We use autoionization rates of autoionizing energy levels in Fe²³⁺ from Autostructure (Badnell 2011). The list of autoionization rates for the energy levels near Fe XXV $K\alpha$ energies is given in Table 1.

3. Simulation Parameters

For our simulation with CLOUDY, we use the temperature, metal abundance, and turbulence in Perseus core. Although the hydrogen column density reported by Hitomi Collaboration et al. (2018a) ($N_{\rm H} \sim 1.88 \times 10^{21}\,{\rm cm}^{-2}$) is too small in Perseus to show the effect of RAD, we extend our parameter space up to a hydrogen column density $N_{\rm H} = 10^{25}\,{\rm cm}^{-2}$. This is to document models of optically thick environments to which CLOUDY can

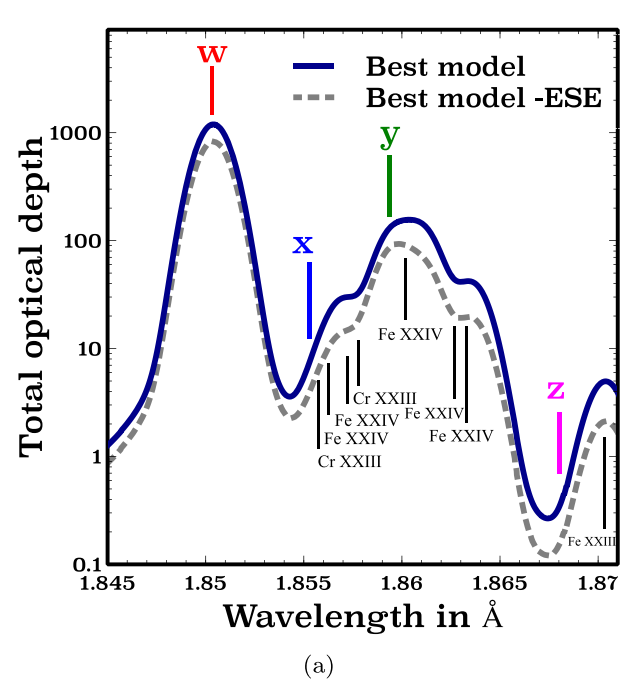
be applied. We choose the temperature and Fe abundance in the interval $4.05^{+0.01}_{-0.01}$ keV and $0.65^{+0.01}_{-0.01}$ of solar, respectively, following the Hitomi observations (Hitomi Collaboration et al. 2018b) from a broadband fit in the energy range 1.8–20.0 keV. We assume an average hydrogen density of $0.03 \, \mathrm{cm}^{-3}$ in our region of interest, and a chromium to iron abundance ratio ~ 0.15 . Although the Hitomi Collaboration et al. (2018b) reported a slight difference in turbulent broadening between w (159–167 km s⁻¹) and x, y, z (136–150 km s⁻¹) in the outer core of Perseus, we use a turbulent velocity of 150 km s⁻¹ in our simulation for simplicity.

4. Loss of Identity via "Line Interlocking"

The total optical depth of the cloud determines the radiative transfer effects in line photons like absorption by ions of the same/ different element, or the Case A to B transfer (see Paper II). A photon within a line simply scatters off the total opacity that is present in the gas. It has no knowledge of which transition or species created that opacity. This scattering produces "line interlocking," where a photon can change its identity. This process is described, for instance, in Elitzur & Netzer (1985) and Netzer et al. (1985).

CLOUDY handles line overlap with a "fine opacity" grid that is described by Shaw et al. (2005). The left panel of Figure 1 shows this fine opacity grid in the spectral region near Fe XXV K α for $N_{\rm H}=10^{25}~{\rm cm^{-2}}$, the upper limit of column density used in our calculations. For w, the total line-center optical depth solely comes from its single-line optical depth. But x, y, and z have contributions from other lines. The dominant contributions to the total optical depth at the center of x are from Fe XXIV ($\lambda=1.8571~{\rm \AA}$) and Cr XXIII ($\lambda=1.8558~{\rm \AA}$) satellites, and z is from Fe XXIII ($\lambda=1.8704~{\rm \AA}$). y has a small contribution from the Fe XXIV satellite ($\lambda=1.8610~{\rm \AA}$). ESE also becomes important at such a high column density. The Figure shows the variation of the total line-center optical depth with wavelength for our best model and a model without ESE with solid and dashed lines, respectively.

The right panel of Figure 1 shows the contrast between the single-line and total line-center optical depths of x, y, z, w for our best model, and their variation with column density. The single-line optical depths in x and z significantly differ from that of their line-center optical depths. This difference is a result of absorption of x and z photons by Fe²³⁺ and Cr²²⁺, and Fe²²⁺, respectively, at the wavelengths mentioned in the previous paragraph. The total line-center optical depth in y has



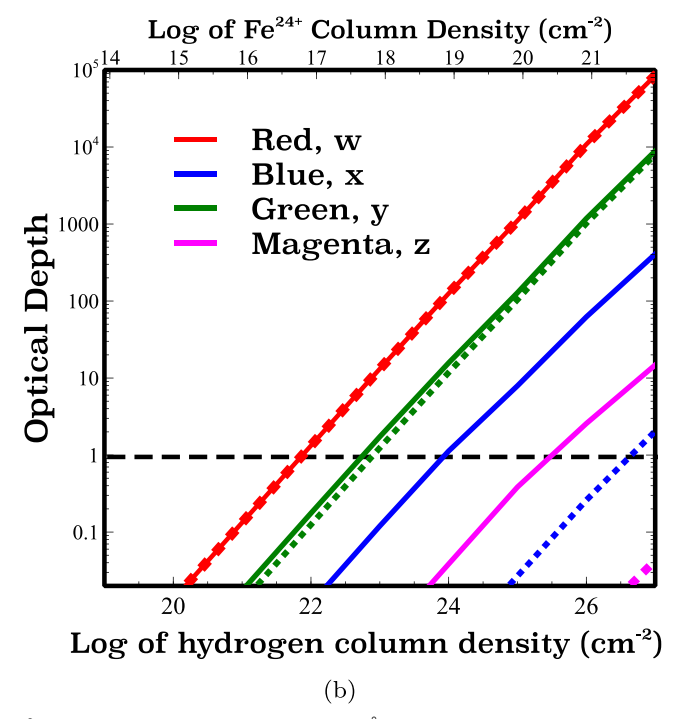


Figure 1. (a) Total optical depth for a cloud with a hydrogen column density of 10^{25} cm⁻² plotted as a function of wavelength in Å. The solid and dashed lines show our best model and the best model without ESE, respectively. The vertical lines above the blue curve mark the wavelengths of w, x, y, and z. Individual lines with a single-line optical depth $\geqslant 1$, are marked with vertical lines below the gray dashed curve. (b) Variation of total line-center optical depth, and single-line optical depth for x, y, z, and w with hydrogen column density for our best model. The solid lines show the total line-center optical depths, and the dashed lines show single-line optical depths for these lines. The slower than linear increase in the total line-center optical depths in x, y, and z photons in the high-column-density limit is due to the decline in the Fe²³⁺ and Fe²²⁺ concentration following autoionization and RAD.

a relatively smaller deviation from its single-line optical depth. This happens due to absorption by Fe²³⁺. There is an overlap between the two optical depths in w as expected, with zero absorption by other ions.

The total line-center optical depth shows a linear increase with column density for w. However, x, y, and z show a slightly slower than linear increase in their total line-center optical depth with column density in the high-column-density limit. Such deviations from linearity are caused by a decline in the Fe^{23+} and Fe^{22+} concentration through RAD (Liedahl 2005). See the next section for further discussion.

5. Autoionization following Absorption

As a direct consequence of "line interlocking", a line photon emitted by one ion can be absorbed by another ion of the same/different element with approximately the same energy. This section discusses the atomic processes following absorption of the lines in the Fe XXV K α complex by various ions, while Section 6 explores the changes in Fe XXV K α line intensities due to the absorption.

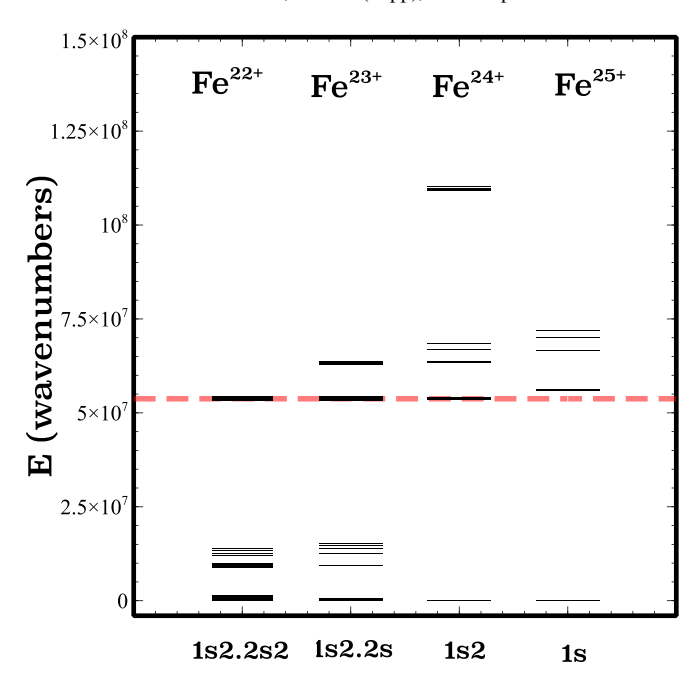
The top panel of Figure 2 shows the energy levels for one-, two-, three-, and four-electron iron. The red dashed line marks the energy of the Fe XXV $K\alpha$ complex. The Figure shows a clear proximity of selected Fe²²⁺ and Fe²³⁺ energy levels to the Fe XXV $K\alpha$ energies. These energy levels lie well above the ionization limits of three-, and four-electron iron, hence they are autoionizing levels. An enlarged version near the Fe XXV $K\alpha$ energies is shown in the bottom panel of Figure 2. An additional column showing the energy levels in Cr^{22+} is included in the enlarged version, as the x line-center optical depth has contributions from a Cr XXIII transition too (see

Section 4). The probability of a Fe XXV K α line photon being absorbed by other ions depends on two factors. The first factor is whether the energy levels of the absorbing ion are similar enough to the emitted line photon to allow line interlocking. The bottom panel of Figure 2 gives a visual illustration of the proximity in energy levels in different ions. The second factor is if the optical depth for that transition is large enough for the absorption to happen, where optical depth is given by the equation:

$$\tau_{\nu}(x) = 2.24484 \times 10^{-14} A_{u,l} \lambda_{\mu m}^3 \frac{g_u}{g_l} \frac{\varphi_{\nu}(x)}{u_{\text{Don}}} N_{\text{ion}}.$$
 (1)

Once absorbed, the excited ion may or may not undergo autoionization. The probability of autoionization depends on the following ratio: $p_a = \frac{A_a}{(A_a + A_{u,l})}$, where A_a is the autoionization rate of the upper level of the excited ion, and $A_{u,l}$ is the downward radiative transition probability. For light elements like helium, p_a is usually close to 1. In heavier elements like iron, p_a can be as small as $\sim 10^{-5}$ for some levels. Table 1 gives the list of $A_{u,l}$, and A_a for the Fe XXV K α energies, and the list of $A_{u,l}$ for Fe²⁴⁺ generating the Fe XXV K α complex.

The total x line-center optical depth becomes $\geqslant 1$ only for hydrogen column densities— $N_{\rm H} \geqslant 10^{24}\,{\rm cm}^{-2}$. The transition wavelengths in the proximity of x ($\lambda=1.8554\,{\rm \AA}$) are: two Fe XXIV ($\lambda=1.8563\,{\rm \AA}$, 1.8571 Å), and one Cr XXIII ($\lambda=1.8558\,{\rm \AA}$) satellite lines. Among these, one of the Fe XXIV satellites ($\lambda=1.8563\,{\rm \AA}$) has a negligible contribution in the absorption of x due to its small $A_{u,l}$ (see Table 1). The transitions dominating absorption of x are therefore Fe XXIV ($\lambda=1.8571\,{\rm \AA}$), and Cr XXIII ($\lambda=1.8558\,{\rm \AA}$). The former has



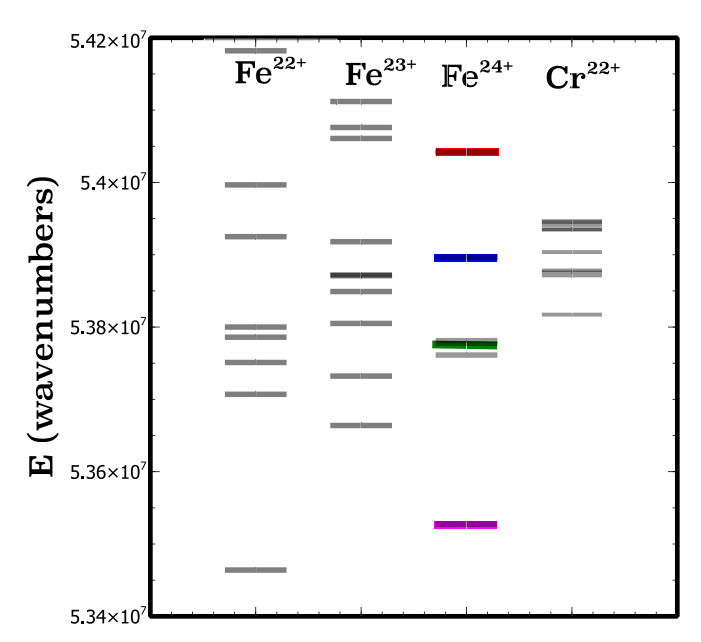


Figure 2. Top: partial energy level diagram of one-, two-, three-, and four-electron iron. The red dashed line marks the energy of the Fe XXV $K\alpha$ complex. Bottom: enlarged energy diagram of Fe^{22+} , Fe^{23+} , Fe^{24+} , and Cr^{22+} near Fe XXV $K\alpha$ complex. Red, blue, green, and magenta lines mark the upper energy level of the w, x, y, and z transition.

 $p_a=0.29$, while the latter has $p_a\sim 10^{-2}$ for one scattering. Therefore, in the instances of a single absorption by Fe²³⁺ corresponding to $\lambda=1.8571\,\text{Å}$, approximately one-third of Fe²³⁺ will autoionize, destroying the absorbed x photons, and causing a deficit in the x line intensity. If absorbed by Cr²²⁺, the ion will most likely de-excite through the emission of a line photon of the same wavelength, having no effect on the x line intensity.

In contrast, the line-center optical depth in y ($\lambda=1.8595\,\text{Å}$) has a small contribution from the Fe XXIV satellite at the wavelength 1.8610 Å with $p_a\sim10^{-5}$. Even though a small fraction of y is absorbed by Fe²³⁺, the autoionization

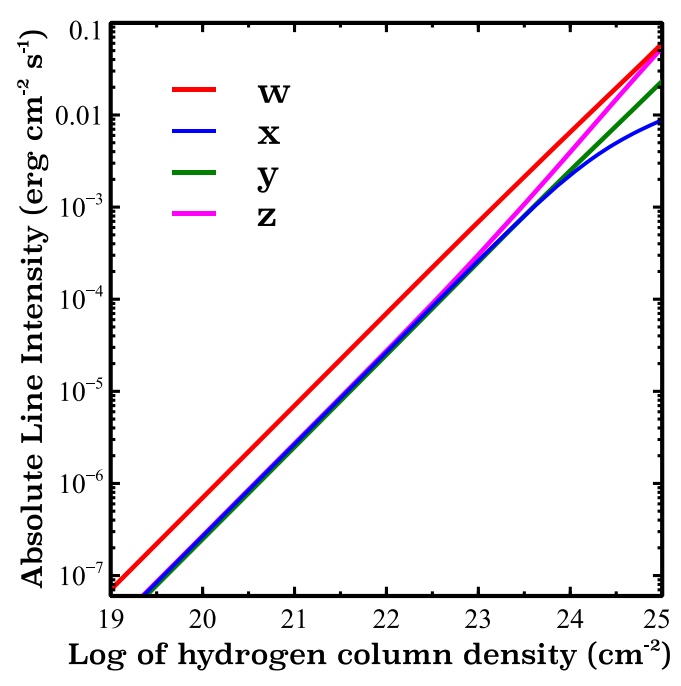


Figure 3. Absolute line intensities for the members of the Fe XXV $K\alpha$ complex with respect to hydrogen column density.

probability is negligible. Up to very high column densities $(N_{\rm H} \le 10^{25}~{\rm cm}^{-2})$ the line-center optical depth in z remains <1. Thus, the absorption of z photons ($\lambda=1.8682~{\rm \AA}$) does not become important despite its proximity to the Fe XXIII satellite line at $\lambda=1.8704~{\rm \AA}$. Beyond this column density, however, some z photons will be absorbed by Fe²²⁺, with a very small probability of autoionization and loss of z photon ($p_a \sim 10^{-2}$).

The loss of line photons following autoionization is referred to as RAD in Ross et al. (1996) and Liedahl (2005). This not only leads to suppression of selective line intensities in the high column density (see the next section) but also causes the absorbing ion concentration to decrease due to autoionization. The higher the p_a , the higher the number of RAD and the more pronounced this effect will be. That is why the x line-center optical depth shows a clear slower-than-linear growth in the high column density range $(N_H \ge 10^{24} \, \text{cm}^{-2})$ in the right panel of Figure 1, while y only slightly deviates. In the very high column density $(N_H \ge 10^{25} \, \text{cm}^{-2})$, line-center optical depth in z shows a slight slower-than-linear growth due to absorption by Fe²²⁺, following RAD.

6. Spectroscopic Evidence of RAD

The continuous increase in the line intensities with column density makes it difficult to detect where the redistribution in photon energy is happening via absorption/re-emission (see Figure 3). Such effects can be best demonstrated with a lineratio diagnostic instead.

We plot the variation of x, y, z line intensities relative to w versus hydrogen column density in Figure 4. As the total-line-center optical depth in w comes entirely from its single-line optical depth, absorption by other ions does not have any effect on its line intensity. The amount of change in the line ratios of x, y, and z relative to w will therefore only be subject to the change in the numerator intensities due to absorption by ions.

In the low-column-density limit, all the lines in the Fe XXV $K\alpha$ complex are optically thin. Line photons emitted in the

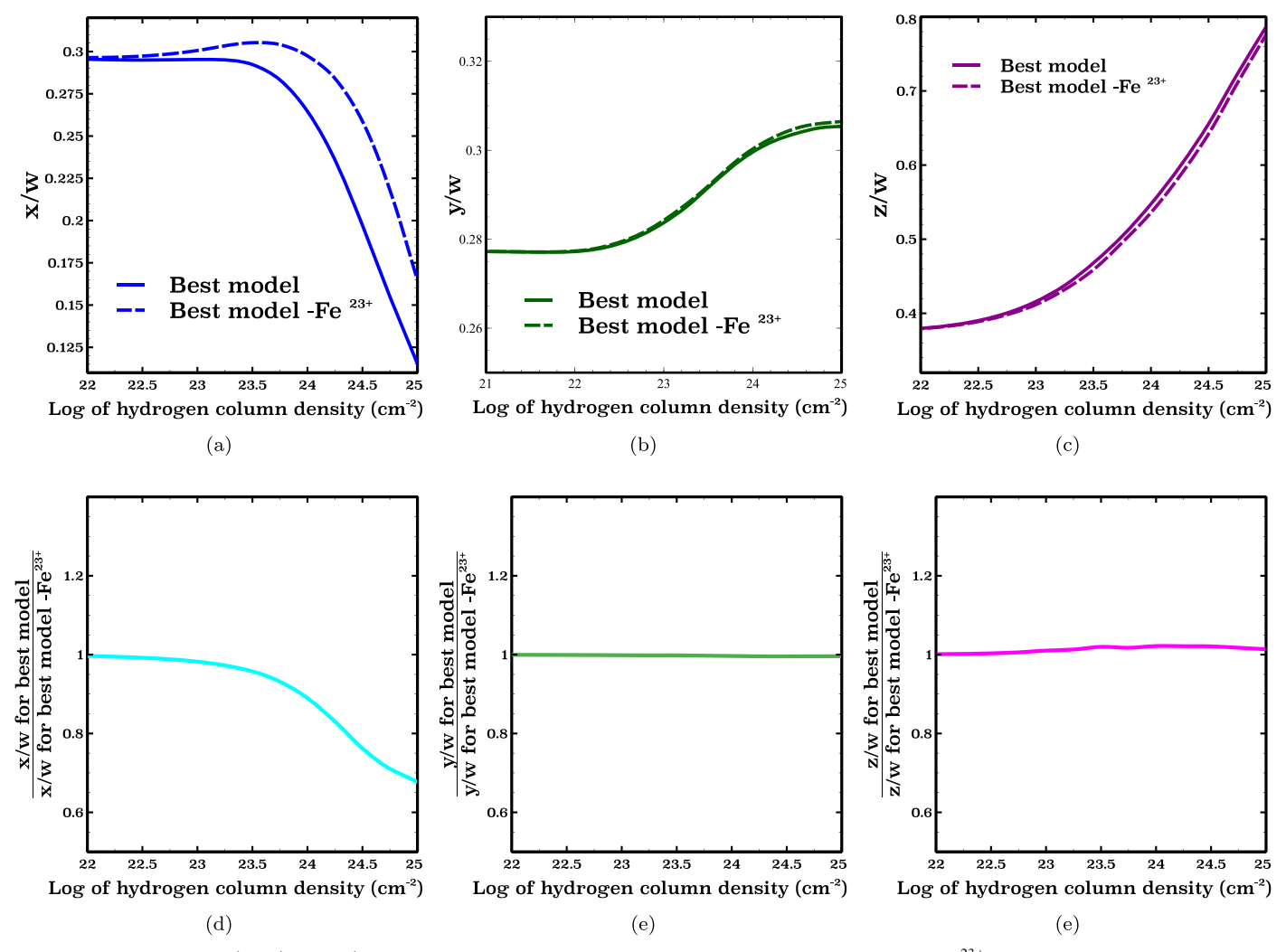


Figure 4. Top: variation of x/w, y/w, and z/w with hydrogen column density for our best model, and a model excluding Fe^{23+} . Bottom: variation of the ratios of our best model to the model without Fe^{23+} for x/w, y/w, and z/w with hydrogen column density.

cloud escape. Without absorption by ions, the line intensities increase with column density. The line ratios, therefore, remain unchanged in the low-column-density limit. In the high-column-density limit, two atomic processes simultaneously change the line intensities of the Fe XXV $K\alpha$ complex: absorption of line photons following line interlocking, and the transfer from Case A to B. The former is studied in this paper, while the latter is the subject of the accompanying paper (Paper II). Additionally, in the very high-column-density limit $(N_{\rm H} \geqslant 10^{23} \, {\rm cm}^{-2})$, ESE also starts to become important.

Section 4 discussed the contribution of absorption by Fe^{23+} in deciding the line-center optical depth in x and y. CLOUDY normally determines the population of various ion stages self consistently. To test the role of Fe^{23+} , we artificially set the abundance of Fe^{23+} to a very small value and compare it with an all-ion-inclusive model. The top panel of Figure 4 compares the x/w, y/w, and z/w ratios with and without Fe^{23+} .

The top left panel of the Figure compares the x/w ratios with and without Fe²³⁺. The change in the x line intensity for our best model (with Fe²³⁺) comes from the Case A to B transition, line interlocking with Fe²³⁺, and ESE (see Section 7), and other factors mentioned in the appendix. The Case A to B transition causes all $2 \rightarrow 1$ line intensities, and therefore the line ratios, to increase (see Section 6.2 in Paper II). We find the

increase in x/w due to Case A to B transfer to be small. The decrease in the x/w ratio with column density in the Fe^{23+} inclusive model is partly due to interactions with Fe^{23+} . As w is not affected by Fe^{23+} , the decrease in the x/w line ratio in the presence of Fe^{23+} only reflects the deficit in x line photons at the higher column densities. According to our calculations, $\sim 32\%$ of x photons are lost due to absorption by Fe^{23+} at the hydrogen column density 10^{25} cm⁻².

Analytically, the fraction of photons destroyed due to RAD depends on the downward radiative transition probability $(A_{u,l})$, and autoionization rate of the upper level (A_a) . When the x photon is absorbed by Fe²³⁺, corresponding to the wavelength 1.8571 Å, the fraction of x photons destroyed in one scattering is $p_a = \frac{A_a}{(A_a + A_{u,l})} = 0.29$, as discussed in the previous section. The optical depth contribution at the line center of x due to line interlocking with the $\lambda = 1.8571$ Å transition is \sim 1 at the hydrogen column density of 10^{25} cm⁻². This implies that \sim 29% of the x photons are destroyed at $N_{\rm H} = 10^{25}$ cm⁻². The analytical theory of RAD is therefore consistent with our calculation, which predicts a 32% deficit in x line intensity at the same hydrogen column density.

For the sake of simplicity in the demonstration, we compare the analytical and calculated values for the decrease in x line intensity

due to RAD at the hydrogen column density 10^{25} cm $^{-2}$. RAD in x, however, begins at a much lower hydrogen column density $(N_{\rm H}=10^{23}~{\rm cm}^{-2})$. The percentage of x photons destroyed at the hydrogen column densities $10^{23}~{\rm cm}^{-2}$, $10^{24}~{\rm cm}^{-2}$, $10^{25}~{\rm cm}^{-2}$ are $\sim 2\%-3\%$, $\sim 12\%$, and $\sim 32\%$, respectively. The bottom panel of Figure 4 shows the variation of the ratios of x/w, y/w, and z/w for our best model to the model without Fe²³⁺ with hydrogen column density.

The upper middle panel of Figure 4 compares the y/w ratio for our best model and a model excluding Fe²³⁺. Unlike x, the presence of Fe²³⁺ slightly alters y line intensity ($\leq 2\%$). This is expected, as the line-center optical depth in y has a much smaller contribution from Fe XXIV ($\lambda = 1.8610 \, \text{Å}$), with $p_a \sim 10^{-2}$. The slight increase in y/w in the high column density happens due to Case A to B transfer and will be addressed in Paper II.

The right panel of Figure 4 compares the z/w ratio with and without Fe²³⁺. As the presence of Fe²³⁺ does not make z optically thick even at our highest column density limit $(N_{\rm H}=10^{25}\,{\rm cm}^{-2})$, ideally z line intensity should remain the same for the with or without Fe²³⁺ models. However, both plots in the right panel show a small increase in the z/w ratio (~2%) in the presence of Fe²³⁺. This behavior is the opposite of that of x/w indicating that the number of x photons lost is converted to z photons causing z/w to increase in the Fe²³⁺ model. This is the Case A to B behavior discussed in detail in Paper II, and points toward the conversion of a tiny fraction of x photons into z photons.

7. Electron Scattering Escape

7.1. General Formalism

The mean number of scatterings (N) experienced by a line photon before escaping an optically thick cloud is related to its line-center optical depth (τ) with the following equation (Ferland & Netzer 1979):

$$N = \begin{cases} 1.11\tau^{0.826} & \text{if } \tau < 1\\ \frac{1.11\tau^{1.071}}{1 + (\log \tau / 5.5)^5} & \text{if } \tau \geqslant 1. \end{cases}$$
 (2)

Note that the number of scatterings is nearly linear in τ and is not proportional to τ^2 , as would occur if it did a random walk in space.

Cloudy uses the formalism developed by Hummer & Kunasz (1980) in treating energy loss during resonance scattering. This treatment does apply to Fe K α since the range of damping constants they consider does extend up to the very large values ($a \sim 0.045$ for w) found in allowed X-ray transitions. This theory predicts a modest increase in path length, which is taken into account.

The presence of fast thermal electrons in the cloud may lead to one-scattering-escape in some fraction of the line photons. This happens when line photons receive a large Doppler shift from their line-center upon scattering off high-speed electrons. The probability of scattering off electrons is given by the following:

$$P_{\text{broad}} = \frac{\kappa_e}{\kappa_{\text{tot}}},\tag{3}$$

where κ_e is the electron scattering opacity, and $\kappa_{\rm tot}$ is the total line-center opacity at that wavelength. $\kappa_{\rm tot}$ includes total line opacity ($\kappa_{\rm line}$) and continuous opacity ($\kappa_{\rm con}$). The latter

includes electron scattering (κ_e), photoelectric absorption, and dust opacity (if dust is present).¹

The fraction of photons escaping the cloud after N scattering is

$$f_{\text{ese}} = 1 - (1 - P_{\text{broad}})^N.$$
 (4)

We name this process of photon escape following a single event of scattering off electrons "ESE."

At the Perseus core temperature, the velocity of an electron is mildly relativistic (\sim 37,200 km s⁻¹), about 15% of the speed of light. The ratio of electron to iron thermal widths is $\sqrt{m_{\rm Fe}/m_{\rm e}} \sim$ 300. When the photons scatter of such high-speed electrons, they are Doppler-shifted far away from the line center and escape the cloud. This leads to the broadening of Gaussian line profiles with a super-broad base under Fe XXV K α of \sim 1 keV width. This is a line broadening process that can be observed only in the high-column-density limit with an optically thick cloud. Therefore, Perseus is not subject to line broadening due to ESE. But optically thick environments such as accretion disks will show such line broadening.

ESE depends on the two following factors: the probability of being scattered by electrons (P_{broad}), and the mean number of scatterings (N) experienced by the line photons (see Equation (4)). The single-line opacities (κ_{line}) in x, y, and z are smaller than that of w. Their P_{broad} values are larger, which makes them more likely to suffer electron scattering. w has a much (\sim 100 or higher) larger mean number of scatterings N, which tends to increase the possibility of ESE; but its much larger κ_{line} makes P_{broad} smaller, which tends to decrease ESE. This complex interplay between N and P_{broad} causes changes in the line profiles in x, y, z, and w. However, this does not change the line intensities in x, y, z, or w. The Gaussian line profiles get broader and flatter due to ESE, keeping the area under the Gaussian and the intensity constant. We show the ratio of total line intensities under the Gaussians in Figure 5. The line intensities (and the line ratios), although independent of ESE in x, y, z, and, w, depend on the following factors:

First, ESE in other line photons can cause the line intensities in x, y, z, and w to change. Figure 5 compares the line ratios with respect to w with and without ESE for the following cases: (a) in an all-ion-inclusive model /our best model, and (b) for a model excluding Fe²³⁺. In the optically thick (Case B) limit, higher n Lyman lines are converted to Balmer plus Ly- α photons, causing an overall increase in the Fe XXV K α complex line intensities (Paper II). Higher-n Lyman lines have smaller $\kappa_{\rm line}$, and thus have a higher probability of being scattered by electrons according to Equation (3). A fraction of the higher-n Lyman lines will therefore escape the cloud through ESE before being converted to Ly α . This will result in a net decrease in the Fe XXV K α complex line intensities, which will weaken the weak $n=2 \to 1$ transitions (x, y, z) more than w, the strongest. This explains the overall

We evaluate Equation (3) assuming that the line opacity does not depend on optical depth. This is equivalent to assuming that the opacity does not depend on frequency. This is true for electron scattering since the Klein–Nishina cross section varies very slowly with energy. The $K\alpha$ line opacity has an energy dependence given by the Voigt function. Lines that scatter in the core of the profile undergo a complete redistribution where the absorbed and emitted photon energy is uncorrelated. This leads to a frequency-independent source function that is constant across the Doppler width. Thus, to a fair approximation, we can evaluate the line opacity and assume that the ratio given in Equation (3) does not depend on optical depth. We know of no numerical calculations of transport of strongly damped lines with background opacity, other than Hummer & Kunasz (1980), which considers only larger optical depths. Such calculations should be done in support of future microcalorimeter missions.

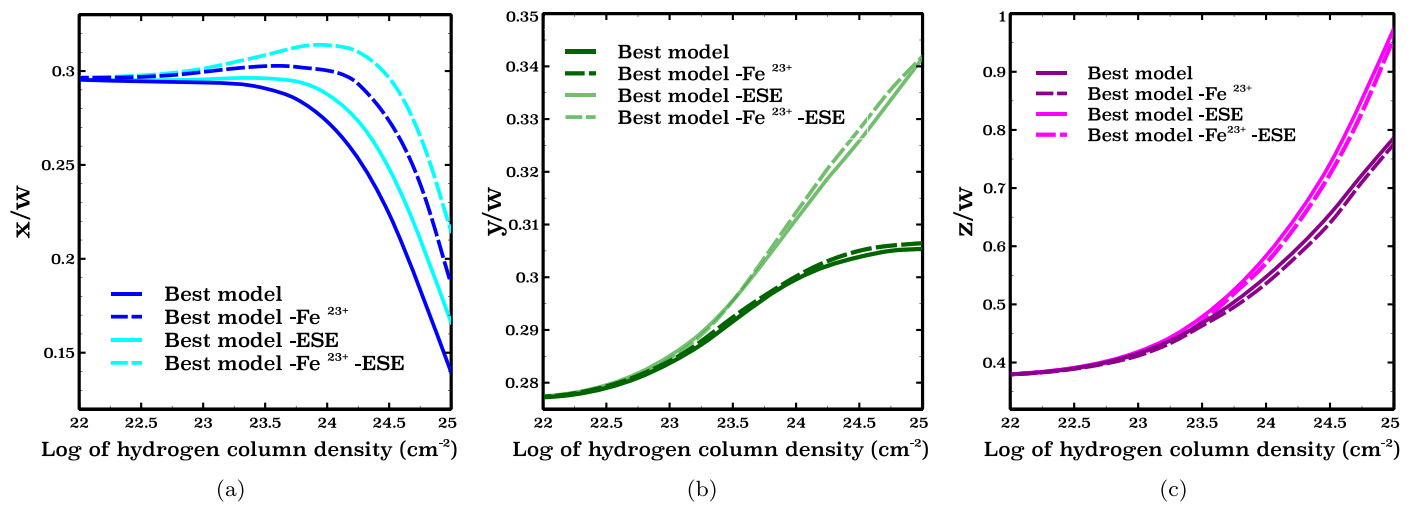


Figure 5. Left, middle, and right panels show the variation of x/w, y/w, and z/w with respect to the hydrogen column density for our best model and a Fe²³⁺ exclusive model, with and without ESE. The best model consists of a narrow line component and a broad line component coming from ESE.

decrease in x/w, y/w, and z/w line ratios in Figure 5 in the presence of ESE.

Second, the presence of ESE can slightly increase the line intensity in x. The x photons that escape the cloud following electron scattering will not be subject to absorption by Fe^{23+} . Thus ESE in x photons reduces the effect of RAD on x line intensity. This implies that the intensity of x line photons in our best model including ESE will be slightly enhanced compared to the without ESE model. The line intensity change in Fe XXV $K\alpha$ complex due to ESE is collectively determined by the ESE of higher n Lyman line photons and weakening of RAD effects in x photons. Figure 5 reflects all these contributions.

Note that our best model in the figure calculates line intensities including the super-broad base under the Gaussian. Each Gaussian in our best model consists of two components. A broad line component generated from ESE, and a narrow-line component for the photons not scattered away from the line center. A high-resolution X-ray telescope will only detect the narrow line component. But a low-resolution telescope with a resolution equivalent to 1 keV will detect the narrow and broad line components together. The difference in telescope resolution will therefore detect different line fluxes in the Fe XXV $K\alpha$ complex. In the next subsection, we discuss the variation of line ratios with column densities for the narrow line component, as a high-resolution X-ray telescope will observe it.

7.2. What Will Be Observed?

From the view of high-resolution X-ray spectroscopy, like Chandra HETG, or future observations by XRISM or Athena, photons that suffer ESE are lost from the Fe XXV $K\alpha$ complex. Figure 6 shows the line ratios that will be observed in high resolution. This is different from Figure 5, which included the electron-scattered Fe XXV $K\alpha$ photons and the super-broad base of the Gaussian in the calculation of line intensities (and line ratios).

Let us analytically estimate the reduction in w line intensity in the observed high-resolution spectra due to the migration of w photons away from its line center, following ESE. The probability (P_{broad}) that w suffers ESE and is lost from the observed spectra is given by Equation (3). The probability that the w photons will be emitted as a sharp/narrow w line is given by: $P_{\text{narrow}} = 1/N$ (N is

calculated from Equation (2)). This narrow line intensity will be detected in the high-resolution spectra. At $N_{\rm H}=10^{25}\,{\rm cm}^{-2}$, we find that $P_{\rm broad}\sim 5\times P_{\rm narrow}$. This implies that the observed w line intensity at $N_{\rm H}=10^{25}\,{\rm cm}^{-2}$ should be 5 times smaller than its optically thin limit where the line photons are not subject to ESE. The increase in x/w, y/w, and z/w in Figure 6 partly comes from this reduction of w intensity in the observed high-resolution spectra. The net variation in the line ratios in the Figure is also partly due to a reduction in x, y, and z intensity in the high-resolution observed spectra, and other factors contributing to the line intensity change explained in Section 7.1.

8. Summary

This paper discusses the significance of three-electron iron in deciding the line intensities of the Fe XXV $K\alpha$ complex. We explore the effects of RAD with CLOUDY initially motivated by the Perseus cluster. We extend our analysis to the wide range of column densities we encounter in astrophysics to which CLOUDY can be applied. We summarize our results below:

1. Whether a line photon escapes the cloud without scattering or is absorbed by ions of the same/different elements depends on its line-center optical depth. The total line-center optical depth corresponding to a transition can entirely come from that transition itself or may have contributions from other transitions of the same/ different element. A photon within a line scatters off due to the total opacity, with no knowledge of which transition or species created that opacity. This leads to line interlocking with the possible loss of identity of the absorbed photon. Among the four members in the Fe XXV K α complex, the x line-center optical depth has significant contributions from single-line optical depths of selected Fe XXIV ($\lambda = 1.8571 \,\text{Å}$), and Cr XXIII $(\lambda = 1.8558 \,\text{Å})$ satellites in very high column densities. y and z have contributions from Fe XXIV($\lambda = 1.8610 \,\text{Å}$), and Fe XXIII ($\lambda = 1.8704 \,\text{Å}$) satellites, respectively. The line-center opacity in w is the same as its single-line opacity, and hence is unaffected.

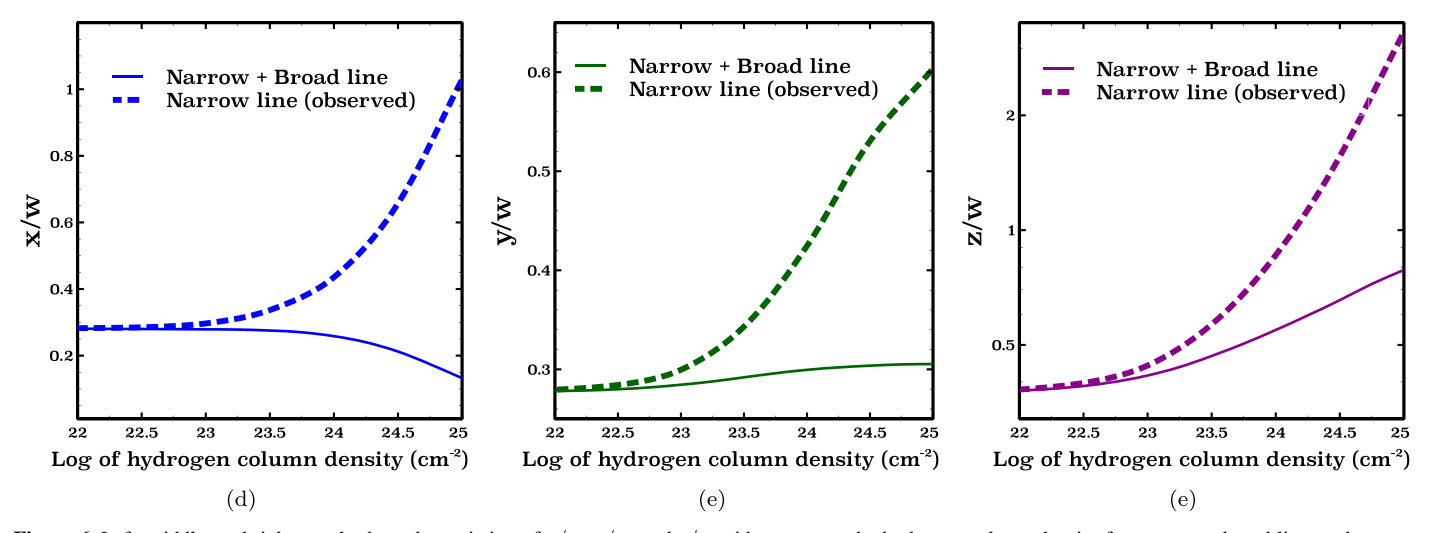


Figure 6. Left, middle, and right panels show the variation of x/w, y/w, and z/w with respect to the hydrogen column density for narrow + broad line, and narrow line components. The total effective intensity of the lines in the Fe XXV K α complex (and the line ratios) consists of the narrow + broad line component and is the same as the best model shown in Figure 5. The broad line component comes from ESE and has a spread of \sim 1 keV. The narrow line component does not include the photons scattered by electrons and is the only line component detected by microcalorimeter/ high-resolution X-ray telescopes. The low-resolution telescopes will detect the narrow and broad line components together.

- 2. Upon absorption by Fe^{23+} , x photons excite Fe^{23+} to the autoionizing level $1s.2s(^3S).2p\ ^2P_{1/2}$ (corresponding to $\lambda=1.8571\ \text{Å}$). Theoretically, $\sim 29\%$ of the x photon should be destroyed in one scattering/ for the optical depth of unity due to RAD. Our calculations show very good agreement with theory. At the hydrogen column density of $10^{25}\ \text{cm}^{-2}$, the optical depth contribution at the line center of x from line interlocking with $\lambda=1.8571\ \text{Å}$ transition is ~ 1 . At the same hydrogen column density, we see a deficit of $\sim 32\%$ in the x line intensity in the presence of Fe^{23+} compared to the case with Fe^{23+} removed for our best model. The change in x line intensity due to RAD, however, begins at a much lower hydrogen column density ($N_{\rm H}=10^{23}\ \text{cm}^{-2}$). The percentage of x photons destroyed at the hydrogen column densities $10^{23}\ \text{cm}^{-2}$, $10^{24}\ \text{cm}^{-2}$, and $10^{25}\ \text{cm}^{-2}$ are $\sim 2\%-3\%$, $\sim 12\%$, and $\sim 32\%$, respectively.
 - A small fraction of y photons excite Fe^{23+} from the ground state to $1s.2s(\,^3S).2p\,^2P_{3/2}$ ($\lambda=1.8610\,\text{Å}$), but rarely get destroyed in RAD, because the autoionizing rate of the excited level is $\sim 10^{-5}$ times smaller than the downward transition probability. z photons do not exhibit line interlocking with any Fe XXIV photons, therefore the z line intensity is not directly affected by RAD.
- 3. Line photons can become heavily Doppler-shifted from their line center after scattering off fast thermal electrons that are present in the cloud. This leads to one-scattering escape for a fraction of line photons, a process we call ESE. Line broadening through this process becomes very important at high column densities. In the high-columndensity limit, ESE can lead to a super-broad base under Fe XXV k α of \sim 1 keV width. The effective intensity of each line in the $K\alpha$ complex consists of a narrow line component and a broad line component coming from ESE. High-resolution X-ray telescopes like XRISM and Athena will only detect the narrow line component, whereas low-resolution telescopes will detect both the narrow and broad line components. The line fluxes detected by high- and low-resolution telescopes will therefore be different.
- 4. Line interlocking processes are very sensitive to line wavelengths. A change of $\sim 0.02\%$ in the wavelengths can significantly alter the line interlocking processes, as well as the nature of line intensities of Fe XXV K α complex. In addition, the optical depth of a line with similar energy as that of Fe XXV K α complex determines the degree of interlocking, making the accurate reporting of transition probabilities in the various atomic data sets extremely important. We found a swap in the transition probabilities between the two Fe XXIV lines ($\lambda =$ 1.8563 Å, $\lambda = 1.8610 \,\text{Å}$) in NIST. A swap in the transition probabilities will significantly change the x line-center optical depth, and change the hydrogen column density to $10^{24} \, \mathrm{cm}^{-2}$ where we see a $\sim 50\%$ decrease in x intensity due to RAD. We verified this mistake with the NIST team, and use CHIANTI version 9.0 instead for both wavelengths and transition probabilities in our calculation.
- 5. Although we assume a static geometry in this paper, we point out that the physics of RAD provides a diagnostic indicator of velocity gradients. The left panel of Figure 4 shows a deficit of ~32% in x line intensity in the presence of Fe²³⁺ due to RAD, as compared to the without Fe²³⁺ case. In our calculations for a static geometry, the artificial removal of Fe²³⁺ from our model negates the effects of RAD. But in a dynamic cloud, a velocity gradient between the Fe²³⁺ and Fe²⁴⁺—emitting regions can also decrease/remove the RAD effects. For instance, if the Fe²³⁺ gas were moving by one or more thermal velocities relative to the Fe²⁴⁺ gas, there will be no overlap and no RAD. Such diagnostics will provide a possible indicator of the velocity gradients.
 6. The ratio of Fe²³⁺-Fe²⁴⁺ abundance depends on the
- 6. The ratio of Fe²³⁺-Fe²⁴⁺ abundance depends on the temperature of the plasma (Nikolić et al. 2013). This ratio is higher in the low-temperature limit. Therefore, the effects of line interlocking and RAD can be observed at much lower column densities in the systems cooler than Perseus. In such systems, there may be significant

- contributions from Fe^{23+} and other satellite lines to what appears to be the x, y, and z.
- 7. Our model assumes a symmetric emitting region, but the combination of asymmetry with the high w line optical depth will increase or decrease w relative to the other lines, as described by Gilfanov et al. (1987), and Paper II.

The comments of John Raymond, the referee of this paper, were very helpful and added significantly to the presentation of our work. His help is gratefully acknowledged. We thank Stefano Bianchi, Andrew Fabian, and Anna Ogorzalek for their valuable comments. We acknowledge support by NSF (1816537, 1910687), NASA (17-ATP17-0141, 19-ATP19-0188), and STScI (HST-AR-15018). M.C. also acknowledges support from STScI (HST-AR-14556.001-A).

Software: CLOUDY (Ferland et al. 2017).

Appendix A The Physics of the x Transition

In the body of the paper, we discussed the effects of Fe^{23+} and ESE in deciding the x/w ratio. However, two other factors change the line intensity in x line interlocking of x with Cr^{22+} and broadband electron scattering (BES). Figure 5 considers the effects of Fe^{23+} and ESE. Figure A1 considers these processes in addition to Cr^{22+} and BES.

The best model is shown in black and discussed above. That discussion also considered the Fe²³⁺ and ESE, which are shown with the red and blue lines. We found that x overlaps with a line of Cr XXIII, which produces additional RAD destruction. This was removed in the green line. Finally, broadband electron scattering traps some line radiation, which produces photoionization, and changes the ionization of the gas. This was removed in the magenta line. Together these processes account for the decrease in x in Figure A1.

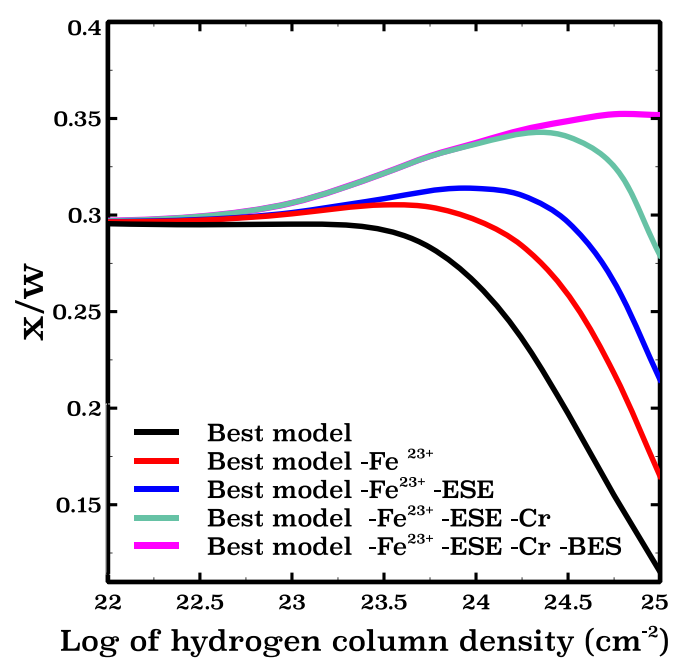


Figure A1. The variation of x/w with hydrogen column density for step-by-step removal of Fe²³⁺, electron scattering escape (ESE), chromium, and broadband electron scattering (BES) from our best model.

Appendix B New CLOUDY Commands

Starting in CLOUDY version 17.03, ESE can be switched off using the command:

no scattering escape physics.

We exclude the effects of ESE in Figure 5 with this command.

In the presence of ESE, there will be a narrow and broad line component in each Gaussian in the Fe XXV K α complex. Only the narrow line components will be detected in the high-resolution

telescopes. The narrow components from each Gaussian can be extracted with CLOUDY using the command

no scattering escape intensity

in the input script. This is a change from the older version of CLOUDY that only had the no scattering escape command.

ORCID iDs

P. Chakraborty https://orcid.org/0000-0002-4469-2518 G. J. Ferland https://orcid.org/0000-0003-4503-6333 M. Chatzikos https://orcid.org/0000-0002-8823-0606 F. Guzmán https://orcid.org/0000-0002-2915-3612

References

```
Badnell, N. R. 2011, CoPhC, 182, 1528
Badnell, N. R., Bautista, M. A., Butler, K., et al. 2005, MNRAS, 360, 458
Band, D. L., Klein, R. I., Castor, J. I., & Nash, J. K. 1990, ApJ, 362, 90
Bautista, M. A., & Kallman, T. R. 2000, ApJ, 544, 581
Bianchi, S., & Matt, G. 2002, A&A, 387, 76
Bianchi, S., Matt, G., Nicastro, F., Porquet, D., & Dubau, J. 2005, MNRAS,
Chakraborty, P., Ferland, G. J., Guzmán, F., & Su, Y. 2020, ApJ, 901, 69,
   (Paper II)
```

Churazov, E., Forman, W., Jones, C., Sunyaev, R., & Böhringer, H. 2004,

MNRAS, 347, 29 Dere, K. P., Del Zanna, G., Young, P. R., Landi, E., & Sutherland, R. S. 2019, ApJS, 241, 22

Dere, K. P., Landi, E., Mason, H. E., Monsignori Fossi, B. C., & Young, P. R. 1997, A&AS, 125, 149

Elitzur, M., & Netzer, H. 1985, ApJ, 291, 464

Ferland, G., & Netzer, H. 1979, ApJ, 229, 274

```
Ferland, G. J., Chatzikos, M., Guzmán, F., et al. 2017, RMxAA, 53, 385
Gilfanov, M. R., Syunyaev, R. A., & Churazov, E. M. 1987, SvAL, 13, 3
Hitomi Collaboration, Aharonian, F., Akamatsu, H., et al. 2016, Natur,
  535, 117
```

Hitomi Collaboration, Aharonian, F., Akamatsu, H., et al. 2018a, PASJ, 70, 12

Hitomi Collaboration, Aharonian, F., Akamatsu, H., et al. 2018b, PASJ, 70, 10 Hummer, D. G., & Kunasz, P. B. 1980, ApJ, 236, 609

Kelley, R. L., Akamatsu, H., Azzarello, P., et al. 2016, Proc. SPIE, 9905, 99050V

Kramida, A., Ralchenko, Y., Nave, G., & Reader, J. 2018, in 49th Annual Meeting of the APS Division of Atomic, Molecular and Optical Physics Meeting (College Park, MD: APS), M01.00004, http://meetings.aps.org/ link/BAPS.2018.DAMOP.M01.4

Liedahl, D. A. 2005, in AIP Conf. Ser., 774, X-ray Diagnostics of Astrophysical Plasmas: Theory, Experiment, and Observation, ed. R. K. Smith (Melville, NY:

Marin, F., Porquet, D., Goosmann, R. W., et al. 2013, MNRAS, 436, 1615 Matt, G., Brandt, W. N., & Fabian, A. C. 1996, MNRAS, 280, 823 Mehdipour, M., Kaastra, J. S., & Raassen, A. J. J. 2015, A&A, 579, A87

Mitchell, R. J., Culhane, J. L., Davison, P. J. N., & Ives, J. C. 1976, MNRAS,

Netzer, H., Elitzur, M., & Ferland, G. J. 1985, ApJ, 299, 752

Nikolić, D., Gorczyca, T. W., Korista, K. T., Ferland, G. J., & Badnell, N. R. 2013. ApJ. 768. 82

Porquet, D., & Dubau, J. 2000, A&AS, 143, 495

Ross, R. R., Fabian, A. C., & Brandt, W. N. 1996, MNRAS, 278, 1082

Ross, R. R., Weaver, R., & McCray, R. 1978, ApJ, 219, 292

Shaw, G., Ferland, G. J., Abel, N. P., Stancil, P. C., & van Hoof, P. A. M. 2005, ApJ, 624, 794

Smith, R. K., Brickhouse, N. S., Liedahl, D. A., & Raymond, J. C. 2001, ApJL, 556, L91

Tzanavaris, P., Yaqoob, T., LaMassa, S., Yukita, M., & Ptak, A. 2019, ApJ,

Yaqoob, T. 2012, MNRAS, 423, 3360

Yaqoob, T., & Murphy, K. D. 2011, MNRAS, 412, 277